

## Article

# Theoretical Stiffness Modeling and Application Research of a Novel Stacked Flexure Hinge

Yonghong Zhang<sup>1</sup>, Chengmin Wang<sup>1</sup>, Shuangquan Tang<sup>2</sup>, You Jiang<sup>1</sup>, Hong Chen<sup>1</sup> and Wenjie Ge<sup>1,\*</sup>

<sup>1</sup> School of Mechanical Engineering, Northwestern Polytechnical University, Xi'an 710072, China; zhangyonghong@nwpu.edu.cn (Y.Z.); wcm@mail.nwpu.edu.cn (C.W.); jyou@mail.nwpu.edu.cn (Y.J.); 1902783064@mail.nwpu.edu.cn (H.C.)

<sup>2</sup> First Aircraft Design Institute of AVIC, Xi'an 710089, China; tangshuangquan@mail.nwpu.edu.cn

\* Correspondence: gwj@nwpu.edu.cn

**Abstract:** This study investigates and designs a novel stacked hinge with low stiffness, large rotation angle, high strength, and length-adaptive functionality. Firstly, based on the large deformation theory of cantilever beams and relevant theories of leaf springs, a stiffness theoretical model for stacked flexure hinges is established. Subsequently, the stiffness theoretical model is further modified by considering the frictional force, aiming to reduce errors. Secondly, a stiffness-testing experimental platform for this flexure hinge is designed to verify the correctness of the theoretical model. Finally, the stacked flexure hinge is applied to the trailing-edge mechanism of a variable camber wing, achieving a deformation target of 15° downward bending of the wing and demonstrating good shape retention, thereby proving the feasibility of the application.

**Keywords:** stacked flexure hinge; large rotation angle; length-adaptive functionality; stiffness theoretical model; variable camber wing



**Citation:** Zhang, Y.; Wang, C.; Tang, S.; Jiang, Y.; Chen, H.; Ge, W. Theoretical Stiffness Modeling and Application Research of a Novel Stacked Flexure Hinge. *Aerospace* **2023**, *10*, 636. <https://doi.org/10.3390/aerospace10070636>

Academic Editor: Sebastian Heimbs

Received: 5 June 2023

Revised: 5 July 2023

Accepted: 7 July 2023

Published: 14 July 2023



**Copyright:** © 2023 by the authors. Licensee MDPI, Basel, Switzerland. This article is an open access article distributed under the terms and conditions of the Creative Commons Attribution (CC BY) license (<https://creativecommons.org/licenses/by/4.0/>).

## 1. Introduction

As one of the most important components of compliant mechanisms, flexure hinges are widely used in the fields of micro-electro-mechanical systems [1–3], aerospace [4–6], and high-precision measuring instruments [7–9] due to their advantages such as no assembly required, no lubrication needed, friction-free operation, and high precision.

The research of flexure hinges can be traced back to the mid-1960s. Paros [10] was the first to propose the formula for calculating the stiffness of arc-shaped flexure hinges. Lobontiu et al. [11] introduced a rounded-edge flexure hinge and derived the closed-form equation for this flexure hinge using Castigliano's second theorem. Bona et al. [12] proposed a coupling parameterization method based on finite element analysis models to optimize the design of a flexure hinge. The method optimizes the flexible hinge at the geometric level, meaning that the topological structure of the hinge cannot be optimized. Zhu et al. [13] proposed a topology-optimization-based design method for flexure hinges, which can use topology optimization to obtain optimal configurations of flexure hinges. Currently, the state-of-the-art topology-optimization formulas face challenges in terms of usability, generality, implementation complexity, and computational costs when it comes to the design of compliant hinges. Liu et al. [14] designed a novel multi-cut flexure hinge using the topological optimization method and derived the dimensionless empirical equation of the flexure hinge based on the finite element results. As a result, there is a lack of a universally accepted formula [15].

Liu et al. [16] proposed for the first time a generalized design method for three-cross spring flexure hinges and improved the rotational accuracy of the flexure hinges using the sheet displacement constraint. Du et al. [17] proposed a high-precision fully symmetric multi-cross spring flexure hinge based on TRIZ's innovative principle. Zhao et al. [18] carried out accurate modeling and analysis of multi-beam curved flexure hinges in view of the

shortcomings of straight-beam flexure hinges, such as motion incoordination. Tian et al. [19] developed, based on Castigliano's second theorem, the dimensionless empirical equations for the filleted V-shaped, cycloidal, and circular flexure hinges and proved that relatively large deformations and a high rotational accuracy can be achieved. Tseytlin et al. [20] presented equations for the closed form of a single-piece flexure hinge with circular and elliptical cross-sections. The inverse conformal mapping of circular approximation contours was used to derive the analytical solution. Schotborgh et al. [21] used finite element analysis to show dimensionless design diagrams for three typical circular, corner-rounded, and cross-bent hinges. These diagrams can be used as design tools to determine the optimal geometry for compliant mechanism design. Meyer et al. [5] proposed a woven FRP-PACS cantilever flexure hinge that could be applied to deformed flaps. Ling et al. [22] proposed a U-like flexure hinge based on Castigliano's second theorem and calculus theory, and four different flexure hinges were obtained by changing the structural parameters. Circular, elliptical, and leaf springs are currently widely used types of compliant hinges. However, they have some conflicts and drawbacks in terms of output compliance, motion precision, rotation angle, and stress levels [23]. The cross-axis hinge offers both a relatively high precision and range; however, it is unable to support large loads [24]. However, there are still some problems with applying the above flexure hinges to variable camber wings. For example, rigid hinges cannot accommodate large bending or torsional deformations in the wings and are not conducive to lightweight design. Flexure hinges in the form of bending beams have a relatively small range of deformation, and the design needs to consider the bending characteristics of the materials to avoid stress concentration and fatigue issues. Straight-beam-type flexure hinges may experience local stress concentration during deformation, especially near the connection points of the straight beams. Notch-type flexure hinges, due to stress concentration near the thinnest part of the notch, have higher local stress that limits deflection.

In this study, a flexure hinge with length-adaptive functionality was designed to address the issues of high stiffness, limited rotation angle, and motion inconsistency in conventional flexure hinges. Based on the theory of large deflections of cantilever beams and the theory of leaf springs, a theoretical stiffness model for the flexure hinge was derived and modified by considering the frictional force, aiming to reduce errors. Experimental validation was conducted using a stiffness-testing experimental platform, and the hinge was applied to a variable camber wing to demonstrate the correctness and feasibility of the proposed stacked flexure hinge design.

## 2. Design Principles and Analysis of Stacked Flexure Hinge

### 2.1. Principle and Geometric Diagram of Stacked Flexure Hinge

The schematic diagram of a stacked flexure hinge is shown in Figure 1, which consists of three main components: the hinge upper cover, the hinge lower cover, and the stacked spring sheets. A profile diagram of the stacked spring sheet is shown on the right. The hinge upper cover and hinge lower cover are connected to the stacked spring sheets, where the angle adjustment arc is designed to allow an initial installation angle when connected to the mechanism and the clamping shaft is designed as a semicircular shaft for ease of assembly.

To investigate the large deformation of stacked flexure hinges, the stacked spring sheets and the hinge lower cover from Figure 1 are extracted, as shown in Figure 2. The main structure includes a fixed axis with a radius of  $R$ , two clamping axes with a radius of  $r$ , and the stacked spring sheets. In the diagram,  $\alpha$  and  $\beta$  represent the central angles of the arc segments corresponding to the radii  $r$  and  $R$ , respectively.  $l_m$  denotes the axial distance between the fixed axis and the clamping axes, while  $l_n$  represents the axial distance between the two clamping axes.  $l_r$  and  $l_R$  correspond to the arc segment lengths of the central angles  $\alpha$  and  $2\pi - 2\beta$ , respectively.

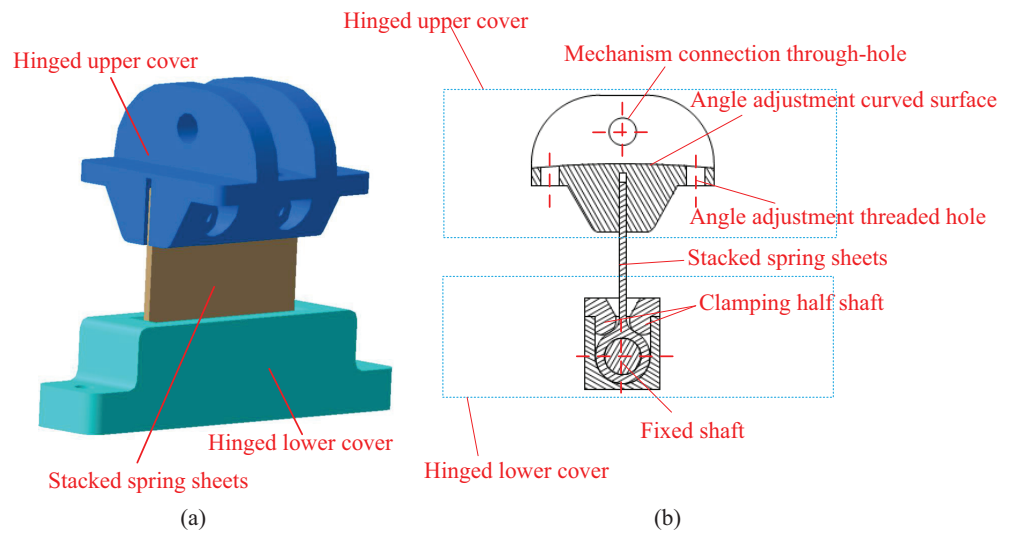


**Figure 1.** Schematic diagram of the stacked flexure hinge. (a) Schematic diagram of the 3D model of the stacked flexure hinge. (b) Stacked flexure hinge cross-section.

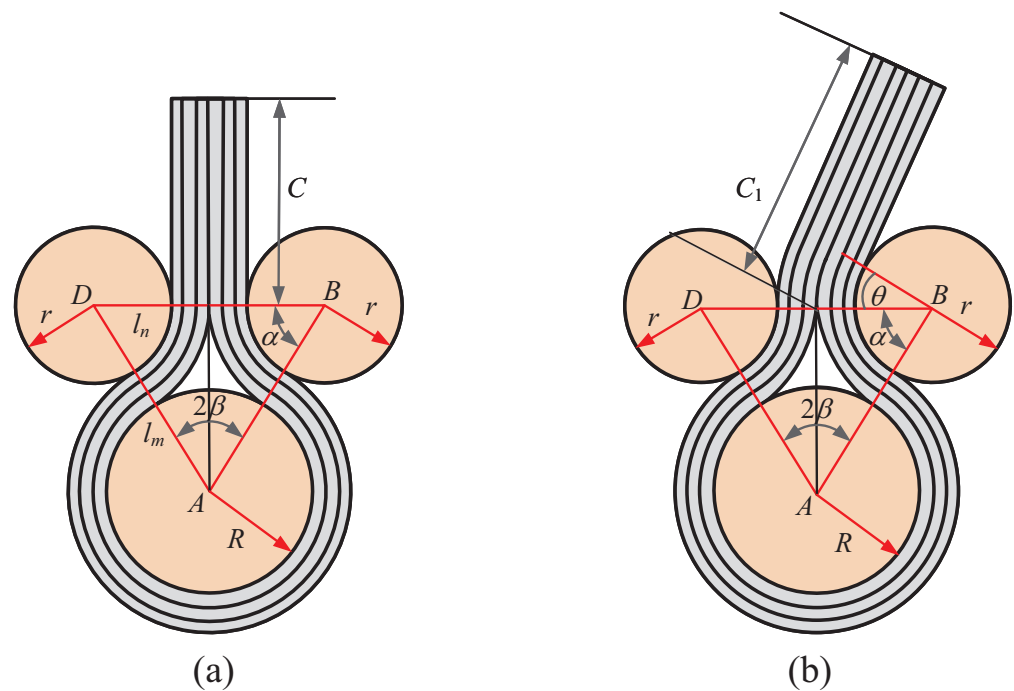


**Figure 2.** Geometric model of stacked flexure hinge. (a) Schematic of the initial state. (b) Schematic of the deformation state.

2.2. Length-adaptive Design and Validation of Stacked Flexure Hinge

Assuming that the flexure hinge consists of  $i$  layers of stacked spring sheets ( $i = 1, 2, 3, \dots$ ), and each layer has a thickness of  $\delta$  mm. Let  $R_j$  represent the sum of  $R$  and the total thickness of the stacked spring sheets and  $r_j$  represent the sum of  $r$  and the total thickness of the stacked spring sheets.  $C$  represents the reserved length of the stacked spring sheets, which is the length of the spring plates below the centerline of the two axes with a radius of  $r$ . Therefore, the relationships among the parameters of the flexure hinge should satisfy the following:

$$l_{ri} = (r + i\delta)\alpha \tag{1}$$

$$l_{Ri} = (R + i\delta)(2\pi - 2\beta) \tag{2}$$

$$l_i = l_{Ri} + 2l_{ri} + 2C \quad (3)$$

In Equation (3),  $l_i$  represents the length of the corresponding layer coil spring in the  $i$ -th layer. The arc length of the  $i$ -th layer coil spring corresponding to the central angle  $\alpha$  can be expressed as:

$$l_{ri} = (\pi/2 - \beta)(r + i\delta) = (\pi/2 - \arcsin(r_i/l_{mi}))(r + i\delta) \quad (4)$$

$$l_{Ri} = 2(\pi - \beta)(r + i\delta) = 2(\pi - \arcsin(r_i/l_{mi}))(r + i\delta) \quad (5)$$

Therefore, the length of the  $i$ -th layer coil spring can be obtained as:

$$l_i = \pi(2R + r + 3i\delta) - \pi \arcsin(r_i/l_{mi})(R + r + 2i\delta)/2 + 2C \quad (6)$$

According to Equation (6), the length of each layer in the stacked spring sheet in the flexure hinge can be calculated.

The following is a proof of the length-adaptive function (the end of the flexure hinge is flush after rotation) of the stacked flexure hinge: assuming that the flexure hinge has  $n$  layers of sheets and  $l_m$  and  $l_n$  are constant, the elongation of the  $i$ -th stacked spring sheets after rotation is expressed as:

$$\Delta l_i = \pi[2r + (i - 1)\delta + (2n - i)\delta]\theta = \pi[2r + (2n - 1)\delta]\theta \quad (7)$$

According to Equation (7), when the structural parameters  $r$  and  $\delta$  of the flexure hinge have been determined, the elongation of each layer of the coil spring is only dependent on the number of layers,  $n$ , and the rotation angle,  $\theta$ . It is independent of the variable  $i$ , which means that the elongation of each layer of the coil spring remains the same after rotation. Since the end of each spring in the flexure hinge is aligned before rotation, when each layer of the coil spring has the same elongation, the end of the flexure hinge will automatically remain aligned after rotation. This proves that the proposed stacked flexure hinge in this paper possesses a length self-adaptive feature and does not exhibit the "bulging" phenomenon.

This section utilizes geometric analysis of the model to deduce formulas for the geometric parameters, including the length of each layer of the stacked spring sheets. It also verifies that the flexure hinge possesses length adaptability. Specifically, during rotation, each spring blade can bend to accommodate changes in the length of the connecting component, allowing the hinge to maintain a stable connection. After rotation, the end automatically aligns itself, preventing serious issues such as rotational center offset. This demonstrates the rationality of the geometric structure of the hinge.

### 3. Stiffness and Strength Analysis of Stacked Flexure Hinge

The large-deformation analysis model of the flexure hinge is illustrated in Figure 3. The flexure hinge is divided into two parts, the left end and the right end, with the axis of the clamping shafts (blue dashed lines) serving as the boundary. Since the left end of the flexure hinge experiences negligible deformation, it is treated as a fixed end, while the right end is considered equivalent to a cantilever beam. In order to facilitate the stiffness calculation of the flexure hinge, the following assumptions are made:

- (1) The deformation of the flexure hinge satisfies the Euler–Bernoulli hypothesis, which states that the equivalent cantilever beam model maintains a perpendicular cross-section to its axis throughout the deformation process.
- (2) The deformation of the flexure hinge only occurs in the right end, and the deformation in other parts is neglected.
- (3) The flexure hinge undergoes bending deformation only, while tensile and shear deformations are disregarded.
- (4) The self-weight of the flexure hinge's stacked spring sheets is negligible.

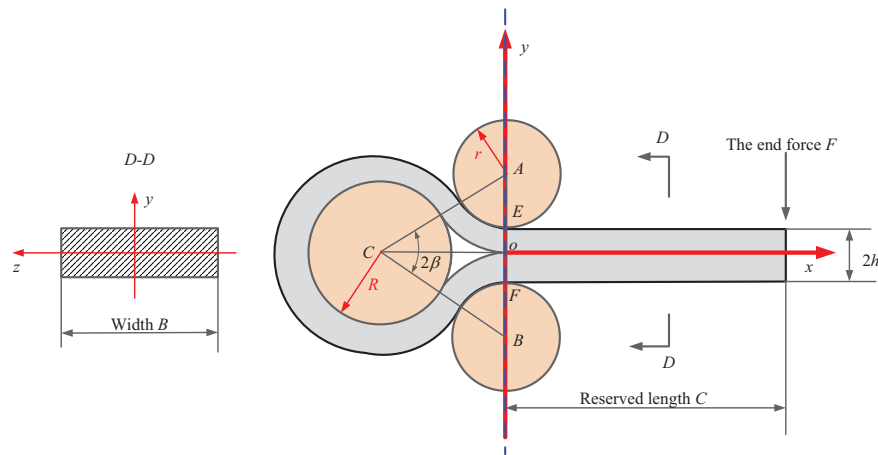


**Figure 3.** Stacked flexure hinge large-deformation analysis model.

To facilitate the analysis, the stiffness theory modeling of small- and large-deformation stacked flexure hinges is carried out in this paper. Under small-deformation conditions, the linear elastic theory can be used for analysis assuming relatively small deformations. This analysis simplifies the calculation process and is applicable to the linear stiffness range of the hinge; when the deformation is larger, the behavior of the hinge may no longer follow the assumption of linear elasticity and nonlinear effects need to be considered. The large deformation analysis is closer to the behavior under actual working conditions. It should be noted that the deformation angle is small when it is less than or equal to  $5^\circ$  and large when it is greater than  $5^\circ$ .

3.1. Small-Deformation Stiffness Analysis of Stacked Flexure Hinge

The differential equation for the small deformation of the cantilever beam can be expressed as:

$$\frac{d^2y}{dx^2} = \frac{M_z(x)}{EI_z} \tag{8}$$

where  $E$  represents the elastic modulus of the cantilever beam and  $I_z$  represents the second moment of inertia of the cantilever beam’s cross-section. The cantilever beam model used in this study assumes a rectangular cross-section, with the second moment of inertia calculated as  $I_z = \rho nB\delta^3 / 12$ . The symbol  $\rho$  represents the inertia section magnification factor, and in this article,  $\rho = 1.5$ .

From Equation (8), the corner function and deflection of the small deformation of the stacked flexure hinge can be obtained as:

$$\begin{cases} \theta = \frac{dy}{dx} = \frac{1}{EI_z} (\int M_z(x)dx + C_1) \\ y = \frac{1}{EI_z} (\int [\int M_z(x)dx]dx + C_1x + C_2) \end{cases} \tag{9}$$

The constants  $C_1$  and  $C_2$  in Equation (9) can be determined by the following boundary conditions:

$$\begin{cases} \theta(0) = 0 \\ y(0) = 0 \\ \theta'(l) = 0 \end{cases} \tag{10}$$

3.2. Large-Deformation Stiffness Analysis of Stacked Flexure Hinge

When stacked flexure hinges undergo a large deformation, meaning a rotation angle greater than  $5^\circ$ , the aforementioned small-deformation theory for cantilever beams is no longer applicable. Therefore, this section derives the large-deformation stiffness model of the stacked flexure hinge based on the cantilever beam large-deformation theory [25] and the plate spring-related theory [26,27] and gives the equivalent analytical model for

the flexure hinge with a cantilever beam, as shown in Figure 4. Introducing the natural coordinate  $s$  to represent the arc length of the cantilever beam and using  $\theta$  to denote the angle of rotation at any point on the cantilever beam, the deflection function of a large deformation of the cantilever beam can be obtained as:

$$\frac{M_z(x)}{EI_z} = \frac{d\theta}{ds} \tag{11}$$

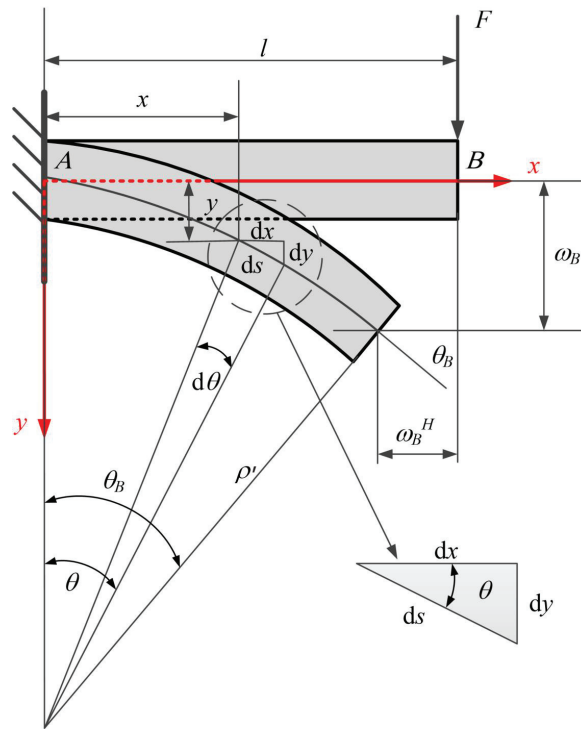


**Figure 4.** The equivalent analytical model for the flexure hinge with the cantilever beam.

According to Figure 4,  $l$  is the total length of the equivalent cantilever beam,  $\omega$  is the deflection at any point on the cantilever beam model,  $\omega_B$  is the deflection at the end of the cantilever beam model, and  $\rho'$  is the radius of curvature. The external force  $F$  acts at the end of the cantilever beam at  $B$ .

$$M_z(x) = -F(l - x - \omega_B^H) \tag{12}$$

Combining Equations (11) and (12), it is obtained that:

$$\frac{d\theta}{ds} = \frac{F}{EI_z}(l - x - \omega_B^H) \tag{13}$$

Take an arbitrary differential unit on the cantilever beam:  $\frac{dx}{ds} = \cos \theta$ ,  $\frac{dy}{ds} = \sin \theta$ ,  $\frac{dy}{dx} = \tan \theta$ . Equation (13) can be expressed as:

$$\frac{1}{2} \left( \frac{d\theta}{ds} \right)^2 = -\frac{F}{EI_z} \sin \theta + C \tag{14}$$

Because  $\left. \frac{d\theta}{ds} \right|_{x=l} = 0$ , so  $\theta(l) = \theta_B$ , where  $\theta_B$  is the end angle of the cantilever beam. Thus, the integration constant  $C$  can be expressed as:

$$C = \frac{F}{EI_z} \sin \theta_B \tag{15}$$

Equation (14) can be rewritten as:

$$\frac{d\theta}{ds} = \sqrt{\frac{2F}{EI_z}(\sin\theta_B - \sin\theta)} \quad (16)$$

Since spring sheet is used as the material for the stacked flexure hinge, its elastic modulus is large and the elongation is small, so the length of the cantilever beam before and after deformation can be considered constant:  $l = l_1$ , so Equation (16) can be rewritten as:

$$\frac{1}{\sqrt{2}} \int_0^{\theta_B} \frac{1}{\sqrt{\sin\theta_B - \sin\theta}} d\theta = \sqrt{\frac{F}{EI_z}} \int_0^{l_1} ds = \sqrt{\frac{F}{EI_z}} l \quad (17)$$

Since the friction between the stacked spring sheets of the flexure hinge and the friction between the individual parts of the stiffness test bench affect the deformation of the flexure hinge, the second moment of inertia section  $I_z$  of the flexure hinge needs to be corrected to obtain a realistic theoretical model of the large deformation of the flexure hinge. The corrected second moment of inertia is represented as  $I'_z$ . Let  $\alpha^2 = Fl^2/EI'_z$  and  $1 + \sin\theta = 2k^2 \sin^2\varphi = (1 + \sin\theta_B) \sin^2\varphi$ . Equation (17) can be rewritten as:

$$\begin{cases} \alpha = \sqrt{\frac{F}{EI'_z}} l = \int_{\omega_1}^{\frac{\pi}{2}} \frac{1}{\sqrt{1-k^2 \sin^2\varphi}} d\varphi \\ \sin\varphi_1 = \frac{\sqrt{2}}{2k} \\ 2k^2 = 1 + \sin\theta_B \\ I'_z = \rho \frac{n(1+\mu)}{12} B\delta^3 \end{cases} \quad (18)$$

where  $\mu$  is the friction coefficient, which is mainly determined by the structural parameters of the flexure hinge and the accuracy of the experimental bench.

### 3.3. Strength Analysis of Stacked Flexure Hinge

In order to ensure the strength and high load-bearing capacity of the stacked flexure hinge, a strength analysis of the stacked flexure hinge is required. The 65 Mn spring sheet with a thickness of 0.1 mm is used as the stacked material of the flexure hinge, and its modulus of elasticity  $E = 196.5$  Gpa and tensile strength  $\sigma_b = 825$  Mpa  $\sim 925$  Mpa, taking into account the safety issue,  $\sigma_b = 825$  Mpa, and setting the safety factor  $S = 2$ . Therefore, the maximum tensile force that the stacked spring sheets of the flexure hinge can withstand is:

$$F_s = [\sigma]A/S = 825 \times B \times 2n\delta/2 = 825Bn\delta \quad (19)$$

where  $A$  is the cross-sectional area of the spring sheet and  $A = Bn\delta$ ;  $[\sigma]$  is the allowable tensile strength of the spring sheet.

When selecting the parameters of the flexure hinge, the number of layers  $n$  and the width  $B$  of the stacked spring sheet required for the flexure hinge can be obtained according to the actual force there. Although multiple solutions can be derived according to Equation (19), not every solution can satisfy the actual working bending deformation. This is because when the bending deformation occurs, the width  $B$  of the stacked spring sheet affects the stability of its deformation, and the smaller the width  $B$  of the stacked spring sheets, the worse its stability; the larger the width  $B$  of the stacked spring sheets, the smaller the number of stacked spring sheets and the lower the fatigue strength of the flexure hinge, so the width of the reed cannot be too large or too small. Considering that the width  $B$  of the stacked spring sheets can have an impact on the bending curvature of the wing's trailing edge during rotation and also affect other structural parameters such as the number of stacks and the reserved length, a comprehensive range of 30–80 mm is recommended for the width.

#### 4. Experiment and Analysis of Stiffness Test of Stacked Flexure Hinge

To verify the correctness of the theoretical model of large deformations of flexure hinges derived above and to improve the generality of flexure hinges, this section conducts a stiffness-test experiment of stacked flexure hinges to investigate the effects of different sheet widths  $B$ , numbers of stacks  $n$ , and reserved lengths  $C$  on the variation in stiffness of stacked flexure hinges.

##### 4.1. Experimental Design for Stiffness Testing of Stacked Flexure Hinge

The design of the stacked flexure hinge stiffness test bench is shown in Figure 5, which mainly includes the experimental platform, the adjustment platform (containing the hinge structure), the stacked spring sheet, the loading pulley, the angle-measuring instrument, the pointer, and the pointer holder. Its working principle is as follows:

- (1) The loading wheel is fixedly connected to the pointer frame by bolts, so the center of rotation of the pointer frame coincides with the center of rotation of the loading wheel and the center of rotation of the flexure hinge;
- (2) A vertical downward force  $F_v$  is applied to the loading wheel, which generates a torque  $M_z$  on the center of rotation of the loading wheel, and this moment will drive the pointer frame to rotate. Since a circular shaft is installed inside the pointer frame and the circular shaft is in contact with the end of the flexure hinge, this moment can be converted into a concentrated force and act on the end of the flexure hinge. This involves the moment balance equation:

$$M_z = F_v r_j = Fh \quad (20)$$

where  $F_v$  is the force applied at the loading wheel,  $r_j$  is the radius of the loading wheel,  $F$  is the concentrated force applied at the end of the flexure hinge, and  $h$  is the vertical distance between the center of rotation of the hinge and the axis of the internal circular axis of the pointer frame.

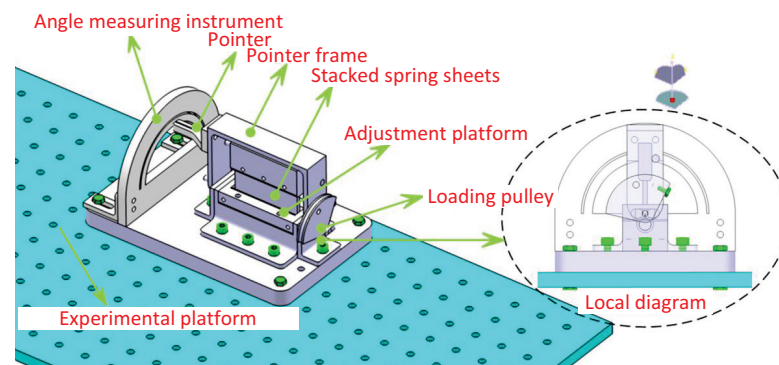


**Figure 5.** Schematic diagram of the experimental platform for stacked flexure hinges.

In the experimental process, due to the different number of stacks of flexure hinges, the installation requirements of flexure hinges with different parameters should be considered when designing the experimental table. Therefore, in this paper, the adjustment platform of the experimental table is designed as a symmetrical U-shaped slot that contains a fixed axis for fixing the stacked spring pieces. The adjustment platform has two clamping axes for clamping the stacked spring and four identical and symmetrical threaded holes on the sides for adjusting the round center distance of the clamping axes.

##### 4.2. Stiffness-Test Experiment of Stacked Flexure Hinge

To verify the correctness of the large-deformation stiffness theory of the stacked flexure hinge, stiffness experiments were conducted in this section for different stacked spring sheet

widths  $B$ , numbers of stacked spring sheets  $n$ , and reserved lengths  $C$ . The experimental schemes of the flexure hinge with different parameters are shown in Tables 1 and 2.

**Table 1.** Experimental scheme of stacked flexure hinges with different numbers of stacks and spring sheet widths.

Parm <sup>1</sup>		B/mm				$\delta$ /mm	C/mm
No.	$n$						
①	$n = 3$	20	30	40	50	0.1	18
②	$n = 4$	20	30	40	50		
③	$n = 5$	20	30	40	50		
④	$n = 6$	20	30	40	50		

<sup>1</sup> Parameters  $n, B, \delta,$  and  $C$  have the same meaning as above and represent the following:  $n$ : number of stacks,  $B$ : width of stacked spring sheets,  $\delta$ : thickness of stacked spring sheets,  $C$ : reserved length.

**Table 2.** Experimental scheme of stacked flexure hinges with different reserved lengths.

Parm		C/mm	B/mm	$\delta$ /mm	$n$
No.					
①		$C = 16$	40	0.1	4
②		$C = 18$			
③		$C = 20$			
④		$C = 22$			

According to Equation (6), to find the initial length  $l_i$  of each layer of spring steel and different widths of spring sheet in order to stack, the installation, loading, experiments, and loading test bench are shown in Figure 6.

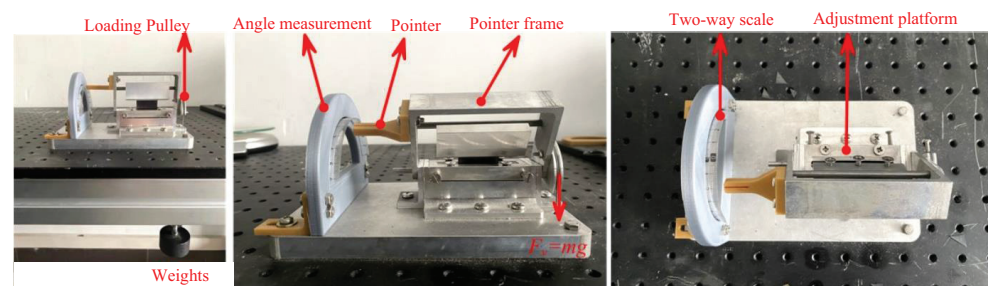


**Figure 6.** Schematic diagram of the stacked flexure hinge loading test.

To reduce the experimental error to ensure the reliability of the data, each group was loaded several times and the average value was used as the corresponding rotation angle for that group. The structural parameters of the flexure hinge and the length of the stacked spring sheets are shown in Tables 3 and 4, respectively. As the stiffness-testing apparatus in this study is equipped with an end-clamping device (which clamps the end portion of the flexure hinge to ensure tight contact between each layer of the spring), the lengths of the spring blades in the table have been appropriately increased (all lengths increased by 4 mm) to ensure that the end-clamping device can grip each stacked layer of the spring tightly.

**Table 3.** Length of each layer of spring sheets of variable-width stacked flexure hinge ( $C = 18$ mm).

Length <sup>1</sup>		$l_1$ /mm	$l_2$ /mm	$l_3$ /mm	$l_4$ /mm	$l_5$ /mm	$l_6$ /mm
No.							
①	$n = 3$	69.87	70.74	71.60	\	\	\
②	$n = 4$	69.87	70.74	71.60	72.47	\	\
③	$n = 5$	69.87	70.74	71.60	72.47	73.32	\
④	$n = 6$	69.87	70.74	71.60	72.47	73.32	74.19

<sup>1</sup>  $l_i$  represents the length of the  $i$ -th spring sheet.

**Table 4.** Thickness of each layer of the spring sheets of the flexure hinge with varying reserved length ( $n = 4$ ).

No.	Length	$l_1/\text{mm}$	$l_2/\text{mm}$	$l_3/\text{mm}$	$l_4/\text{mm}$
①	$C = 16$	65.87	66.74	67.60	68.47
②	$C = 18$	69.87	70.74	71.60	72.47
③	$C = 20$	73.87	74.74	75.60	76.47
④	$C = 22$	77.87	78.74	79.60	80.47

In this paper, the theoretical rotation angle of the stacked flexure hinge is calculated and compared with the experimental rotation angle, and the results are shown in Figure 7; the rotational stiffness of the flexure hinge is calculated based on the loading moment, theoretical rotational stiffness, and experimental rotational stiffness, as shown in Figure 8.

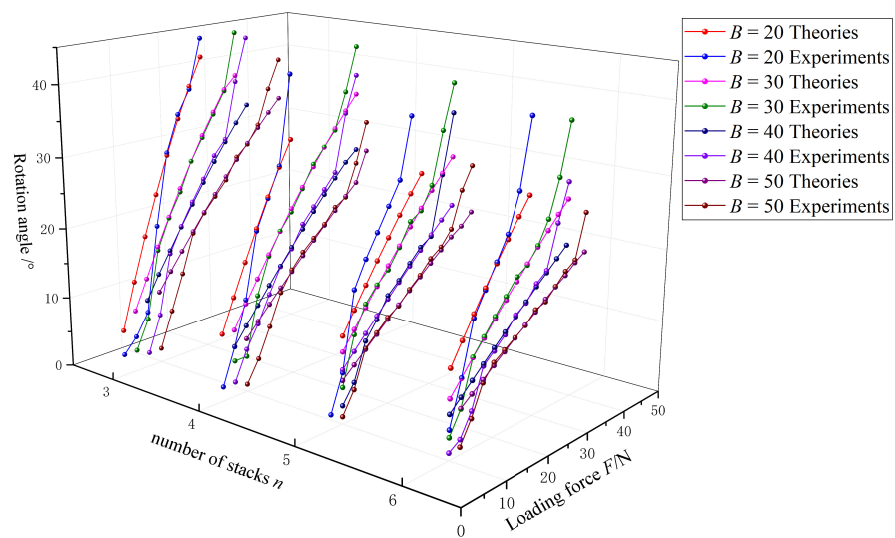


**Figure 7.** Comparative graph of theoretical and experimental results for different widths of spring sheets with number of stacks  $n = 3 \sim 6$ . Relationship between loading force and rotation angle.

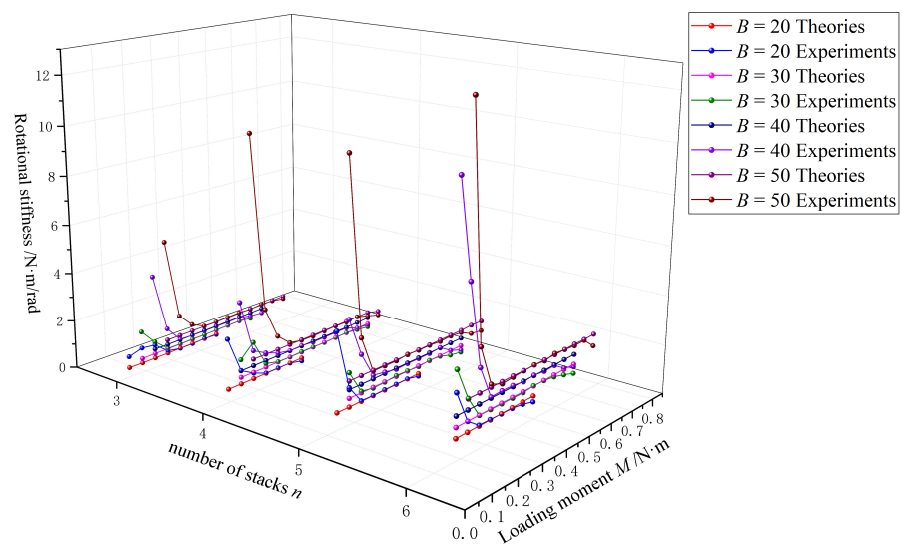


**Figure 8.** Comparative graph of theoretical and experimental results for different widths of spring sheets with number of stacks  $n = 3 \sim 6$ . Relationship between loading moment and rotational stiffness.

Analysis of Figures 7–9 leads to the following conclusions:

- (1) The rotation angle of the stacked flexure hinge is nonlinearly related to the loading force, so it conforms to the large-deformation theory of cantilever beams. With the increase in the number of stacks  $n$  and spring sheet width  $B$ , the flexural capacity of the flexure hinge increases and its deformation tends to be linear; therefore, in order to avoid the nonlinear deformation of the flexure hinge, we can choose a larger number of stacks  $n$  or appropriately increase the spring sheet width  $B$  in the design parameters of the flexure hinge.
- (2) When the number of stacked spring sheets, reserved length, and loading force are the same, the flexural capacity and stability of the flexure hinge increase with the increase in the spring sheet width; under the same width, reserved length, and loading force, the rotational stiffness and load capacity of the hinge increase with the increase in the number of layers of the spring sheet.
- (3) It can be observed that there are some discrepancies between the theoretical results and experimental results when the load force is relatively small or large. When the loading force is small, the deflection angle of the flexure hinge is small due to the friction force between the stacked spring sheets and the influence of the experimental table; when the loading force is large, the flexure hinge overcomes the influence of the friction force and produces a rotation angle that tends to be linear. Therefore, when selecting the parameters of the flexure hinge, attention should be paid to the influence of the friction force between the stacked spring sheets to prevent the occurrence of nonlinear deflection.
- (4) It can be observed that the experimental results do not completely match the theoretical calculations due to limitations imposed by the stiffness-testing apparatus. The longer reserve length of the flexure hinge in this study resulted in a smaller effective utilization range (the range where experimental results and theoretical calculations match). Therefore, for future practical applications, it is advisable to select a smaller reserve length in order to increase the effective utilization range of the flexure hinge.

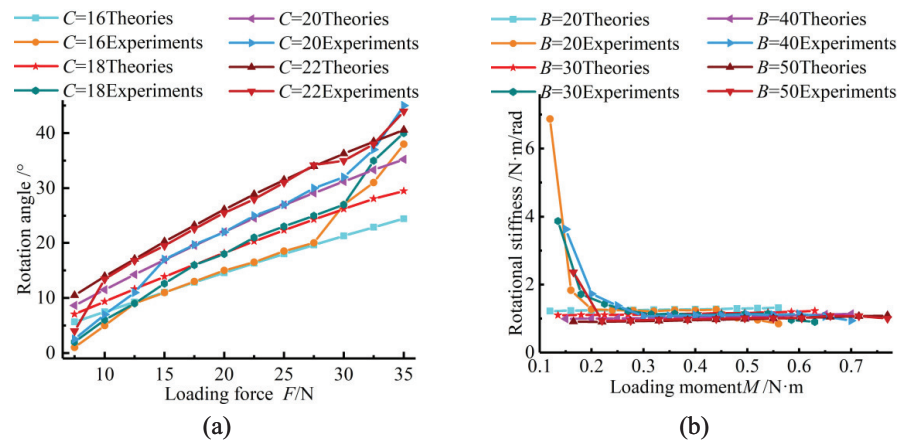


**Figure 9.** Comparative graph of theoretical and experimental results for different reserve lengths of spring sheets with number of stacks  $n = 5$ . (a) Relationship between loading force and rotation angle. (b) Relationship between loading moment and rotational stiffness.

In summary, it can be seen that the large-deformation theory of the cantilever beam is in better agreement with the experimental results, which proves the correctness of the theory of the stacked flexure hinge proposed in this paper. In addition, the number of stacks  $n$  mainly affects the load-bearing capacity of the flexure hinge; the width  $B$  of the stacked spring sheets mainly affects the stability of the flexure hinge; the reserved length  $C$  affects both the load-bearing capacity and the stability of the flexure hinge; and the influence ability is between the number of stacks  $n$  and the width  $B$  of the stacked spring sheets.

#### 4.3. Application of Stacked Flexure Hinges in the Trailing Edge of a Variable Camber Wing

The stacked flexure hinge designed in this paper is mainly used in variable camber wings. In this study, the chord length of the wing's trailing edge is approximately 30% of the total chord length (approximately 4.3 m), which is approximately 1299 mm. For the convenience of wing-loading experiments, the width is designed to be 300 mm. The 1:1 experimental prototype model of the trailing edge of a variable camber wing is shown in Figure 10. Except for the prototype skin, rigid rod hinge shaft, and spring sheets of the stacked flexure hinge, the rest of the parts are made of 6061 aviation aluminum alloy. The skin is made of 3240 epoxy resin glass fiber composite material. The prototype skin is made of glass fiber epoxy composite panel, and the rigid rod hinge shaft is made of 45 steel. Among them, the stacked flexure hinges are all set at the connection between the member and the skin, and the structural parameters of each stacked flexure hinge are shown in Table 5.

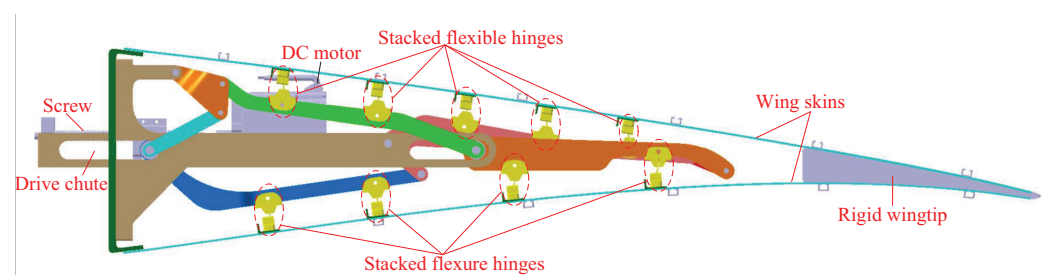


Figure 10. Experimental prototype model of a variable camber flexure wing trailing edge.

Table 5. Structural parameters of stacked flexure hinges.

Parm <sup>1</sup>	No.								
	N <sub>1</sub>	N <sub>2</sub>	N <sub>3</sub>	N <sub>4</sub>	N <sub>5</sub>	N <sub>6</sub>	N <sub>7</sub>	N <sub>8</sub>	N <sub>9</sub>
$\delta/\text{mm}$	0.1	0.1	0.1	0.1	0.1	0.1	0.1	0.1	0.1
$B/\text{mm}$	50	50	80	60	50	50	40	50	40
$n$	6	6	6	6	6	5	5	5	5
$C/\text{mm}$	5.33	5.41	5.15	5	5.02	9	8	7.7	8
$F_{max}/\text{N}$	24,750	24,750	39,600	29,700	24,750	20,625	16,500	20,625	13,200

<sup>1</sup> Parameters  $\delta$ ,  $B$ ,  $n$ ,  $C$  have the same meaning as above. The parameter  $F_{max}$  represents the maximum tensile force.

To achieve the experimental effect of simulating equivalent aerodynamic loads, a loading and alignment system has been designed, with its main components shown in Figure 11. A framework diagram of the wing deformation system is shown in Figure 12. The system consists of a loading system and an alignment system, primarily used for loading, alignment, and directional measurement of the test prototype. The driving system, comprising a power supply, motor, driver, and development board, is responsible for driving the deformation of the test prototype. The data-processing system utilizes a grating displacement sensor for point measurement, collects experimental data, and performs curve fitting.

The aerodynamic load acting on the upper skin is equivalent to six loading forces, while the aerodynamic load on the lower skin is equivalent to five loading forces. These 11 equivalent aerodynamic loads are applied to the upper and lower skins of the test prototype using sandbags and steel wires within the loading system. The alignment system's main function is to keep the equivalent loading forces perpendicular to the skins, as shown in the schematic diagram, Figure 13. It primarily consists of alignment screws and alignment pulleys. To avoid interference between the different equivalent loading forces, the adjustment platform contains three layers of alignment motor screws.

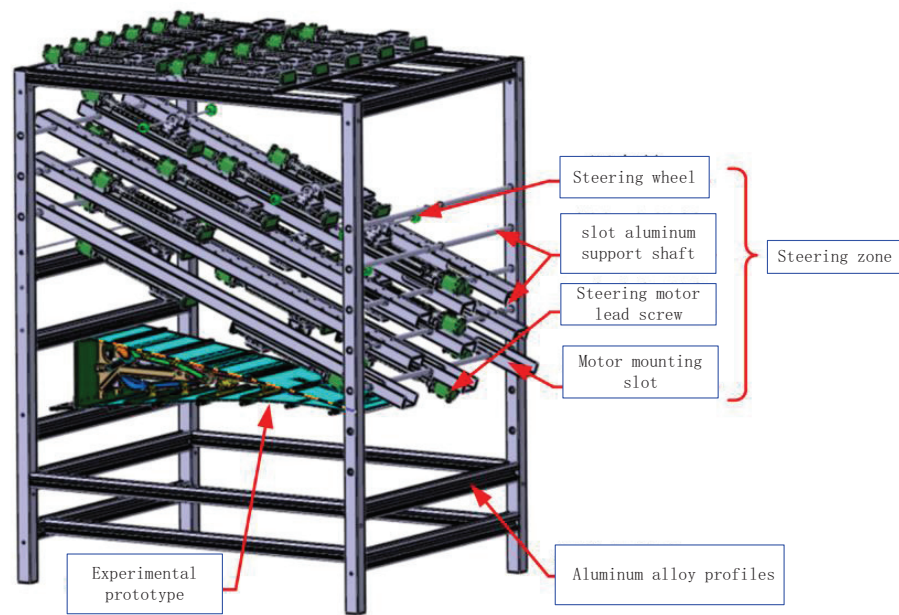


Figure 11. Schematic diagram of the wing-loading experimental setup.

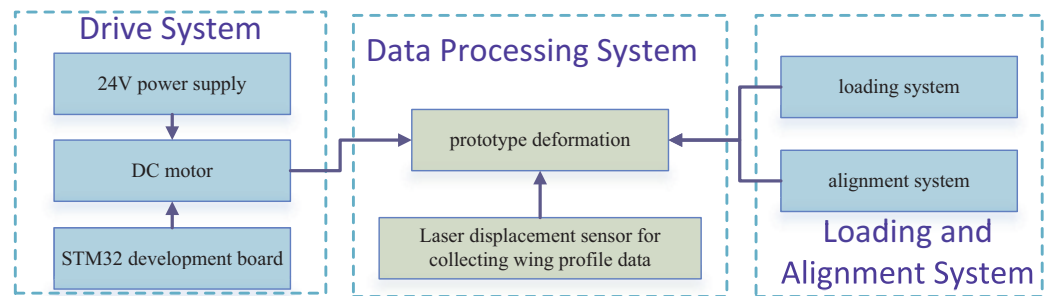


Figure 12. Framework diagram of wing-deformation system.

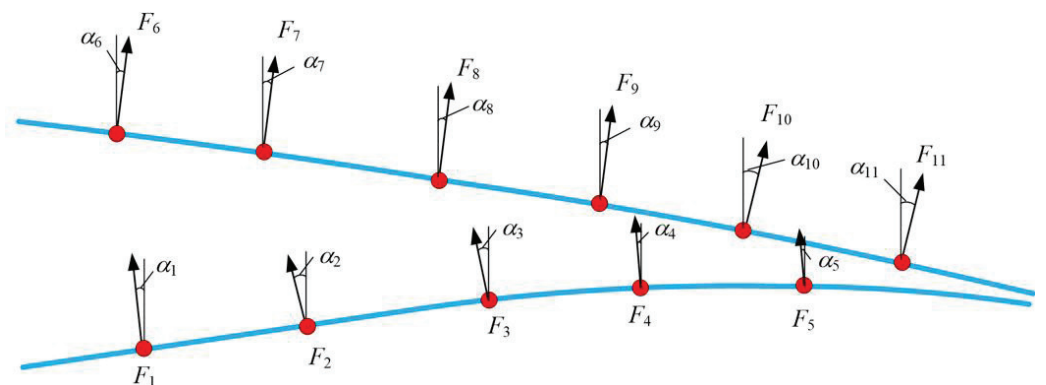
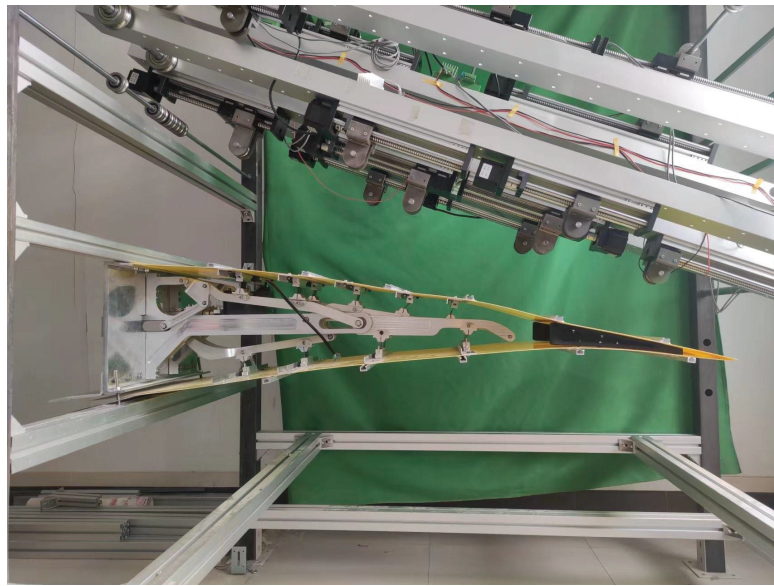


Figure 13. Schematic diagram of equivalent aerodynamic load application.

The test bench is specially designed to simulate the equivalent aerodynamic loads under actual working conditions of the trailing edge of the wing. The parts of the experimental prototype are assembled and installed in the experimental table, and the stacked flexure hinges are installed with an initial angle to create an energy storage effect, the effect is shown in Figure 14.



**Figure 14.** Assembly diagram of the experimental prototype model.

In this paper, a loading experiment of the experimental prototype was conducted, and the effect is shown in Figure 15.

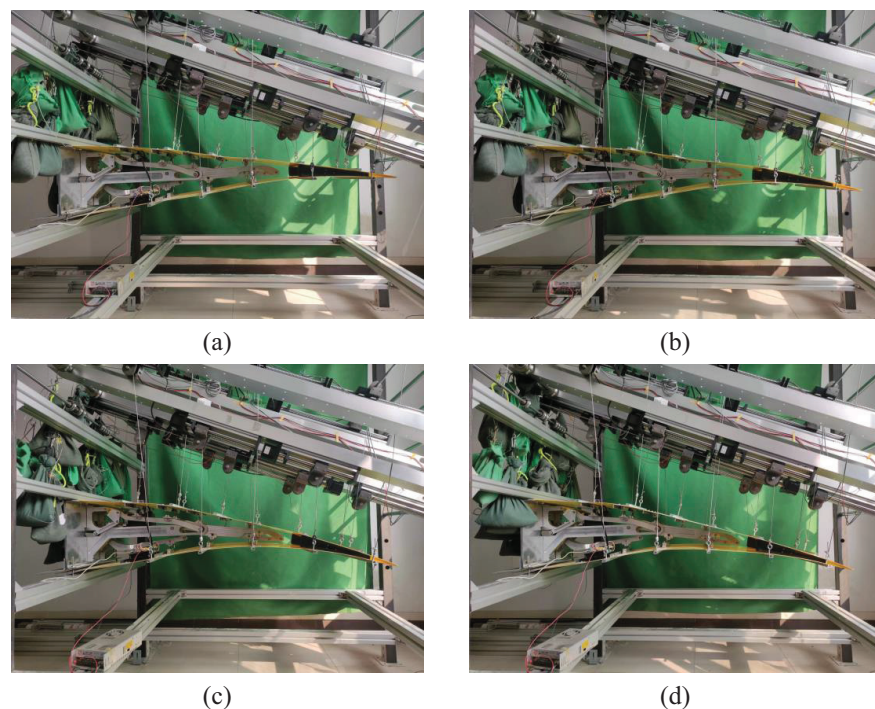


**Figure 15.** Deformation process diagram of the variable camber wing trailing edge under load. (a) Initial Wing Curve. (b) 5° wing curve. (c) 12° Wing Curve. (d) 15° wing curve.

To observe the deformation effect of the experimental prototype, the deformation curve of the experimental prototype is extracted and compared with the deformation curve of the experimental prototype, as shown in Figure 16, where it can be seen that the deformation process of the wing has good conformability. In Figure 17, the 15° deformation curve of the experimental prototype can fit the target deformation curve well, but the loading deformation curve of the experimental prototype still has some errors. The maximum error is about 4.5 mm and the maximum error position is located at the tip of the rigid wing tip.

Through the loading-deformation experiments on the trailing edge of the variable camber wing, it is found that the stacked flexure hinge can effectively solve the problems of poor conformability and low load capacity of the variable camber flexure wing, which verifies the correctness of the stacked flexure hinge theory and the feasibility of applying it to the variable camber flexure wing.

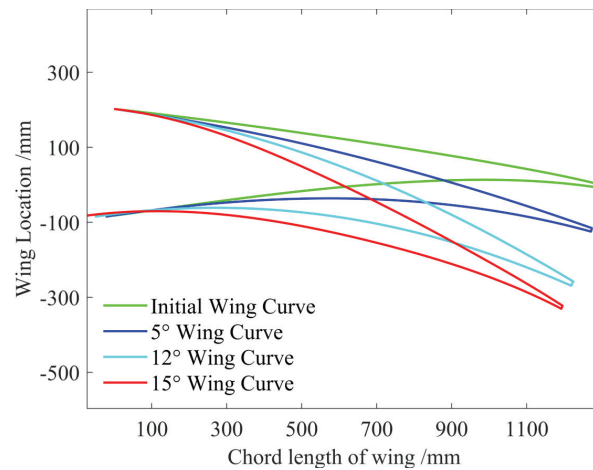


**Figure 16.** Extraction of the airfoil profile curve during the deformation process of the variable camber wing experimental prototype.

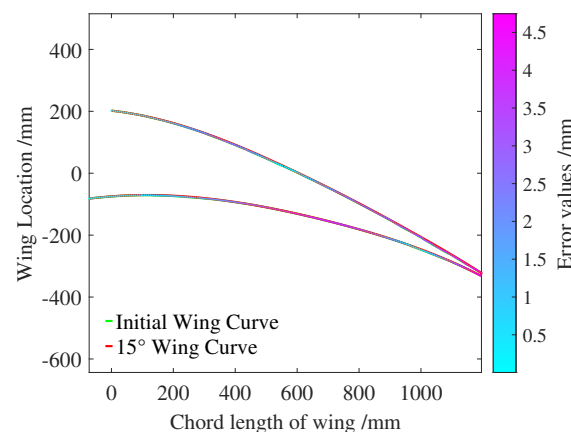


**Figure 17.** Airfoil error during 15° wing deformation of the variable camber wing experimental prototype.

## 5. Conclusions

To improve the load-bearing capacity and shape retention of a flexure wing with variable curvature, this article proposes a novel stacked hinge with a low stiffness, large rotation angle, high strength, and length-adaptive functionality. Firstly, the length-adaptive feature of the flexure hinge is demonstrated through geometric diagrams and relationships. Then, based on the large-deformation theory of cantilever beams, both small-deformation and large-deformation stiffness models are established. The moment of inertia of the cantilever beam cross-section is modified considering frictional forces. Through stiffness-testing experiments, the rotational angle of the stacked flexure hinge is found to have a nonlinear relationship with the loading force, confirming the correctness of the bending hinge's stiffness model. The following conclusions are drawn: the number of layers primarily affects the load-bearing capacity of the flexure hinge, the width of the laminated spring mainly affects the stability of the flexure hinge (effective utilization range), and the reserved length simultaneously affects the load-bearing capacity and stability of the flexure hinge, with its impact lying between the number of layers  $n$  and the width of the laminated spring.

Finally, the novel stacked flexure hinge is applied to a variable-angle wing, and the experimental results of wing deformation demonstrate that the stacked flexure hinge ensures the achievement of the target wing shape, with a maximum error of less than 4.5 mm. It is worth mentioning that due to limitations imposed by the stiffness-testing apparatus, the flexure hinge in this study has a longer reserve length, resulting in a smaller effective utilization range. Therefore, for future practical applications, it is advisable to select a smaller reserve length in order to increase the effective utilization range of the flexure hinge.

**Author Contributions:** Conceptualization, Y.Z. and W.G.; methodology, Y.Z. and C.W.; software, C.W.; validation, S.T., Y.J., and H.C.; writing—original draft preparation, Y.Z., C.W., and S.T.; writing—review and editing, C.W., Y.J., H.C., and W.G.; visualization, Y.Z. and C.W.; supervision, Y.Z.; project administration, W.G.; funding acquisition, W.G. All authors have read and agreed to the published version of the manuscript.

**Funding:** This research was supported by the National Natural Science Foundation of China (No. 51375383).

**Data Availability Statement:** Not applicable.

**Conflicts of Interest:** The authors declare no conflicts of interest.

## References

1. Ma, H.W.; Yao, S.M.; Wang, L.Q.; Zhong, Z. Analysis of the displacement amplification ratio of bridge-type flexure hinge. *Sens. Actuators A Phys* **2006**, *132*, 730–736. [[CrossRef](#)]
2. Zubir, M.N.M.; Shirinzadeh, B.J.; Tian, Y.L. Development of a novel flexure-based microgripper for high precision micro-object manipulation. *Sens. Actuators A Phys* **2009**, *150*, 257–266. [[CrossRef](#)]
3. Kim, Y.S.; Yoo, J.M.; Yang, S.H.; Choi, Y.M.; Dagalakis, N.G.; Gupta, S.K. Design, fabrication and testing of a serial kinematic MEMS XY stage for multifinger manipulation. *J. Micromech. Microeng.* **2012**, *22*, 085029. [[CrossRef](#)]
4. Henein, S.; Spanoudakis, P.; Droz, S.; Myklebust, L.I.; Onillon, E. Flexure pivot for aerospace mechanisms. In Proceedings of the 10th European Space Mechanisms and Tribology Symposium, Technological Park, San Sebastián, Spain, 25 September 2003.
5. Meyer, P.; Boblenz, J.; Sennewald, C.; Vorhof, M.; Hühne, C.; Cherif, C.; Sinapius, M. Development and Testing of Woven FRP Flexure Hinges for Pressure-Actuated Cellular Structures with Regard to Morphing Wing Applications. *Aerospace* **2019**, *6*, 116. [[CrossRef](#)]
6. Jeong, J.W.; Yoo, Y.I.; Shin, D.K.; Lim, J.H.; Kim, K.W.; Lee, J.J.; A novel tape spring hinge mechanism for quasi-static deployment of a satellite deployable using shape memory alloy. *Rev. Sci. Instrum.* **2014**, *85*, 025001. [[CrossRef](#)]
7. Miller, J.A.; Hocken, R.; Smith, S.T.; Harb, S. X-ray calibrated tunneling system utilizing a dimensionally stable nanometer positioner. *Precis. Eng.* **1996**, *18*, 95–102. [[CrossRef](#)]
8. Kim, D.; Kang, D.; Shim, J.; Song, I.; Gweon, D. Optimal design of a flexure hinge-based XYZ atomic force microscopy scanner for minimizing Abbe errors. *Rev. Sci. Instrum.* **2005**, *76*, 073706. [[CrossRef](#)]
9. Choi, S.B.; Han, S.S.; Han, Y.M.; Thompson, B.S. A magnification device for precision mechanisms featuring piezoactuators and flexure hinges: Design and experimental validation. *Mech. Mach. Theory* **2007**, *42*, 1184–1198. [[CrossRef](#)]
10. Paros, J.M. How to design flexure hinges. *Mach. Des.* **1965**, *37*, 151–156.
11. Lobontiu, N.; Paine, J.S.; Garcia, E.; Goldfarb, M. Corner-Filletted Flexure Hinges. *ASME. J. Mech. Des.* **2001**, *123*, 346–352. [[CrossRef](#)]
12. Bona, F.D.; Munteanu, M.G. Optimized Flexural Hinges for Compliant Micromechanisms. *Analog Integr. Circ. Signal Process.* **2005**, *44*, 163–174. [[CrossRef](#)]
13. Zhu, B.; Zhang, X.; Fatikow, S. Design of single-axis flexure hinges using continuum topology optimization method. *Sci. China Technol. Sci* **2014**, *57*, 560–567. [[CrossRef](#)]
14. Liu, M.; Zhang, X.M.; Fatikow, S. Design and analysis of a multi-notched flexure hinge for compliant mechanisms. *Precis. Eng.* **2017**, *48*, 292–304. [[CrossRef](#)]
15. Koppen, S.; Langelaar, M.; van Keulen, F. A simple and versatile topology optimization formulation for flexure synthesis. *Mech. Mach. Theory* **2022**, *172*, 104743. [[CrossRef](#)]
16. Liu, L.; Bi, S.S.; Yang, Q.Z.; Wang, Y.L. Design and experiment of generalized triple-cross-spring flexure pivots applied to the ultra-precision instruments. *Rev. Sci. Instrum.* **2014**, *85*, 105102. [[CrossRef](#)] [[PubMed](#)]
17. Du, S.Y.; Liu, J.N.; Bu, H.Z.; Zhang, L. A novel design of a high-performance flexure hinge with reverse parallel connection multiple-cross-springs. *Rev. Sci. Instrum.* **2020**, *91*, 035121. [[CrossRef](#)]
18. Zhao, H.Z.; Han, D.; Bi, S.S. Modeling and Analysis of a Precise Multibeam Flexural Pivot. *ASME. J. Mech. Des.* **2017**, *139*, 081402.
19. Tian, Y.; Shirinzadeh, B.; Zhang, D.; Zhong, Y. Three flexure hinges for compliant mechanism designs based on dimensionless graph analysis. *Precis. Eng.* **2010**, *34*, 92–100. [[CrossRef](#)]

20. Tseytlin, Y.M. Notch flexure hinges: An effective theory. *Rev. Sci. Instrum.* **2002**, *73*, 3363–3368. [[CrossRef](#)]
21. Schotborgh, W.O.; Kokkeler, F.G.M.; Tragter, H.; Houten, F.J.A.M. Dimensionless design graphs for flexure elements and a comparison between three flexure elements. *Precis. Eng.* **2005**, *34*, 41–47. [[CrossRef](#)]
22. Ling, J.J.; Li, R.Q.; Zhang, Q.S. Flexibility Calculation of Like-U Type Flexure Hinge. *Open Mech. Eng.* **2015**, *9*, 532–539.
23. Ma, W.; Wang, R.Q.; Zhou, X.Q.; Meng, G.W. The performance comparison of typical notched flexure hinges. *Proc. Inst. Mech. Eng. Part C J. Mech. Eng. Sci.* **2020**, *9*, 1859–1867. [[CrossRef](#)]
24. Pinskiar, J.; Shirinzadeh, B.; Ghafarian, M.; Das, T.K.; Al-Jodah, A.; Nowell, R. Topology optimization of stiffness constrained flexure-hinges for precision and range maximization. *Mech. Mach. Theory* **2020**, *150*, 103874. [[CrossRef](#)]
25. Bisshopp, K.E.; Drucker, D.C. Large deflection of cantilever beams. *Q. Appl. Math.* **1945**, *3*, 272–275. [[CrossRef](#)]
26. Childs, P.R.N. 15—Springs. In *Mechanical Design Engineering Handbook*, 2nd ed.; Childs, P.R.N., Ed.; Butterworth-Heinemann: Oxford, UK, 2019; pp. 719–771.
27. Childs, P.R.N. 9—Springs. In *Mechanical Design*, 3rd ed.; Childs, P.R.N., Ed.; Butterworth-Heinemann: Oxford, UK, 2021; pp. 337–370.

**Disclaimer/Publisher’s Note:** The statements, opinions and data contained in all publications are solely those of the individual author(s) and contributor(s) and not of MDPI and/or the editor(s). MDPI and/or the editor(s) disclaim responsibility for any injury to people or property resulting from any ideas, methods, instructions or products referred to in the content.